Fabrication of omentum-based matrix for engineering vascularized cardiac tissues

2014 Biofabrication 6 024101

(http://iopscience.iop.org/1758-5090/6/2/024101)

IOP Publishing Biofabrication
Biofabrication 6 (2014) 024101 (12pp) doi:10.1088/1758-5082/6/2/024101

Fabrication of omentum-based matrix for engineering vascularized cardiac tissues

Michal Shevach[1,2], Neta Soffer-Tsur[1,3], Sharon Fleischer[1,2], Assaf Shapira[1] and Tal Dvir[1,2,4]

[1] The laboratory for tissue engineering and regenerative medicine, Department of Molecular microbiology and Biotechnology, George S. Wise Faculty of Life Science, Tel Aviv University, Tel Aviv 69978, Israel
[2] The Center for Nanoscience and Nanotechnology, Tel Aviv University, Tel Aviv 69978, Israel
[3] Department of Cell Research and Immunology, George S. Wise Faculty of Life Sciences, Tel Aviv University, Tel Aviv 69978, Israel
[4] Department of Materials Science and Engineering, Tel Aviv University, Tel Aviv 69978, Israel

E-mail: tdvir@post.tau.ac.il

Received 26 August 2013, revised 8 October 2013
Accepted for publication 9 October 2013
Published 24 January 2014

Abstract

Fabricating three-dimensional, biocompatible microenvironments to support functional tissue assembly remains a key challenge in cardiac tissue engineering. We hypothesized that since the omentum can be removed from patients by minimally invasive procedures, the obtained underlying matrices can be manipulated to serve as autologous scaffolds for cardiac patches. Here we initially characterized the structural, biochemical and mechanical properties of the obtained matrix, and demonstrated that cardiac cells cultivated within assembled into elongated and aligned tissues, generating a strong contraction force. Co-culture with endothelial cells resulted in the formation of blood vessel networks in the patch without affecting its function. Finally, we have validated that omental scaffolds can support mesenchymal and induced pluripotent stem cells culture, thus may serve as a platform for engineering completely autologous tissues. We envision that this approach may be suitable for treating the infarcted heart and may open up new opportunities in the broader field of tissue engineering and personalized regenerative medicine.

Keywords: cardiac tissue engineering, decellularization, myocardial infarction, omentum, scaffolds

S Online supplementary data available from stacks.iop.org/BF/6/024101/mmedia

(Some figures may appear in colour only in the online journal)

1. Introduction

The inability of the myocardium to heal itself after infarction, and the shortage of cardiac donors, have motivated scientists to explore new technologies for heart regeneration [1]. Cellular therapies, such as intracoronary cell injection, evolved to repopulate the scar tissue with contracting cells. However, lack of control over cell accumulation site, and death of cells before forming interactions with their surroundings have jeopardized the success of such approaches [2–4]. These shortfalls motivated the development of the cardiac tissue engineering concept, where three-dimensional (3D) extracellular matrix (ECM)-like scaffolds are fabricated from biomaterials, providing mechanical support to the assembling tissue.

During the past years various types of biomaterials were used as scaffolds to accommodate cardiac cells, including synthetic (e.g. poly(lactic-co-glycolic acid), poly(glycerol sebacate)) and natural (e.g. collagen, alginate) [5–11]. Although significant improvement in the function of the infarcted heart was reported after implantation of engineered heart patches [8, 12–14], the full therapeutic potential of cardiac tissue engineering has not yet been met. One of

the remaining challenges is the lack of an appropriate microenvironment fostering functional assembly of cardiac tissues [2, 3, 14]. Another drawback is the absence of proper vasculature, which delays the anastomosis with the host post transplantation [13, 15].

In vivo, in addition to mechanical support, the native ECM provides the cells with a wealth of instructive cues for inducing functional tissue assembly [16, 17]. These include topographical signals provided by the intricate mesh of collagens and elastin fibers, adhesion proteins such as fibronectin and laminin, cytokines and growth factors [16]. The latter may be stored by the glycosaminoglycans (GAGs) reservoirs, to be released in a controlled manner into the cell microenvironment, promoting essential physiological processes [16, 18–20].

To supply many of these necessities to the growing cells, various tissues, such as heart valves, blood vessels, urinary bladders, heart muscles and others, were decellularized, and the remaining matrices were used as scaffolds for tissue engineering [21–28]. The significance of naturally derived matrix intrinsic properties in successful cultivation of cardiac cells has led tissue engineers to develop efficient cell removal techniques from pig and rat hearts. The obtained scaffolds had internal fibrillar morphology, inherent vasculature ECM and proper mechanical properties [14, 21, 22, 29]. However, although numerous xenogeneic matrices are available on the market and in clinical use demonstrating biocompatibility, some of these biomaterials may provoke immunogenic response, impairing graft function [28, 30]. In addition, cells isolated from one source may be exposed to an advantageous microenvironment when grown on a matrix isolated from the same individual. In other words, the patient's own cells may grow better on an autologous matrix.

In this study we sought to utilize the omentum matrix as a platform for engineering autologous functional heart tissues with intrinsic vascular network. The omentum is a double sheet of peritoneum that extends from the greater curvature of the stomach overlying most abdominal organs [31]. This tissue is highly vascularized and its fibrillar ECM is rich with collagens, adhesive proteins and GAGs [32, 33]. Due to its unique composition, the omentum also serves as a depot for adult stem cells with regenerative potential [34–36]. These stem cells are based in the omentum matrix and upon signals migrate to heal injured organs [36]. The overall regenerative capacity of the omentum, to maintain progenitor cell viability, absorb large amounts of edema fluids and limit the formation of scar tissue at the site of injury, has long been demonstrated [37–39].

Here, we hypothesized that many of the regenerative properties of the omentum rely in its matrix. Therefore, after efficient cell removal the scaffolding biomaterial can serve as a matrix for cardiac tissue engineering. During many clinical procedures the omentum is removed from patients without health implications [40, 41]. Therefore, we believe that parts of this tissue can be removed by relatively simple microsurgery techniques [42, 43] and further processed to serve as autologous matrices. Such platform can be utilized for engineering personalized cardiac patches. In a recent study the omental tissue was decellularized [44], however, to the best of our knowledge, this is the first study to combine the omental decellularized matrix with cells for the purpose of tissue engineering.

2. Results and discussion

2.1. Assessment of the key factors in the native omental ECM

Prior to the decellularization process we sought to detect the presence of several key factors in the omental tissue, important for engineering vascularized cardiac tissues. These factors include the underlying collagen fibrous mesh, blood vessel infrastructure, adhesion molecules and GAGs.

Masson's trichrome staining of fixed omentum slices revealed high content of collagen fibers (blue) within the tissue, serving as the underlying matrix supporting the cells (figure 1(*a*)). To evaluate the presence of GAGs, fixed slices of omental tissues were stained with Alcian blue. Figure 1(*b*) revealed high content of sulfated GAGs (light blue) throughout the tissue, mainly around blood vessels. Smooth muscle actin staining, which labels smooth muscle cells, revealed a dense vascular network composed of multiple size blood vessels (figure 1(*c*); brown) with high content of vascular endothelial growth factor (VEGF) around them (figure 1(*d*); pink). Analysis of blood vessel density within the omentum revealed 1337 $\pm$ 71 vessels mm^{-2}, which is comparable to the vessel density in the heart 1973 $\pm$ 94 vessel mm^{-2} (supporting information, figure S1, available at stacks.iop.org/BF/6/024101/mmedia). The adhesion molecule laminin was found on the collagen fibers throughout the tissue (figure 1(*d*); green). These parameters have been shown to be essential for functional cardiac tissue assembly [45].

2.2. Decellularization of the omentum and matrix analyses

To evaluate the potential of the omentum matrix to serve as a scaffold for cardiac tissue engineering, we first focused on cell removal. Omental tissues were subjected to various processes (described in detail in the methods section) in order to achieve efficient removal of adipose and blood vessel cells and their fragments (figures 2(*a*)–(*d*)). Complete DNA/RNA removal was validated using Hoechst 33258 staining of ECM and fresh native tissue sections. Nuclei were detected in fresh omentum but not in the decellularized matrix (figures 2(*e*) and (*f*), respectively). Ethidium bromide agarose gel electrophoresis showed no DNA bands associated with the decellularized omental tissue, whereas fresh omentum showed a large band above 9400 bp (figure 2(*g*)). Scanning electron microscope (SEM) analysis performed on native (figure 3(*a*)) and decellularized omentum (figure 3(*b*)) further indicated efficient cell removal and the preservation of a fibrous mesh with blood vessel infrastructure (figure 3(*c*)). Overall, the decellularized matrix contained fibers ranging from 150 nm to several micrometers in diameter (figure 3(*d*)). A matrix composed of such fiber dimensions may serve as an appropriate scaffold for engineering cardiac tissues, as these dimensions are in accordance with the endomysial and perimysial fibers of the native cardiac matrix, wrapping individual cardiomyocytes and cell bundles, respectively [46, 47].

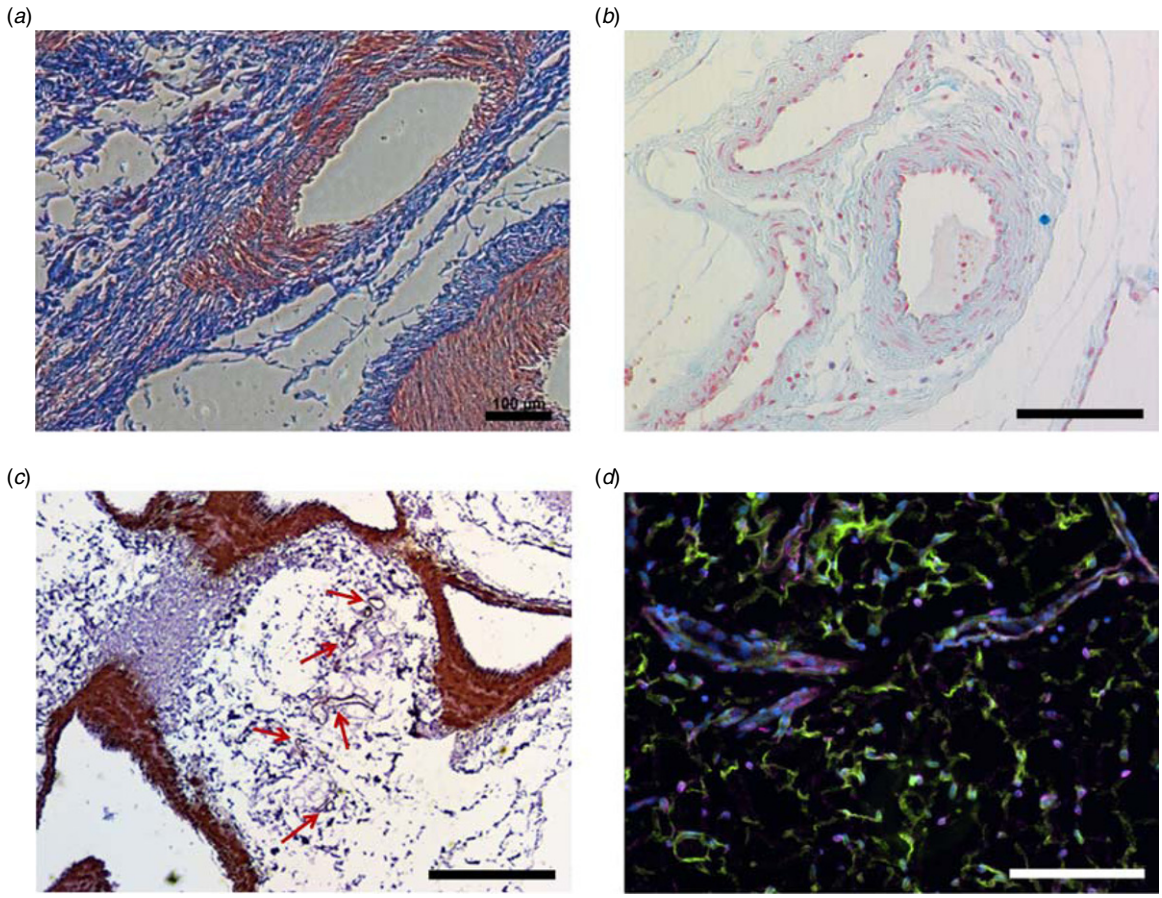

Figure 1. Key factors in the native omental ECM. (*a*) Collagen fibers by Masson's trichrome staining (blue) (*b*). High GAG content throughout the tissue by Alcian blue staining (light blue). (*c*) Smooth muscle actin staining of smooth muscle cells comprising blood vessels (brown, smaller blood vessels are indicated with black arrows). (*d*) Co-staining of VEGF (pink) and the adhesion molecule laminin (green). Bar: $A = 100\ \mu$m, $B = 100\ \mu$m, $C = 100\ \mu$m, $D = 100\ \mu$m.

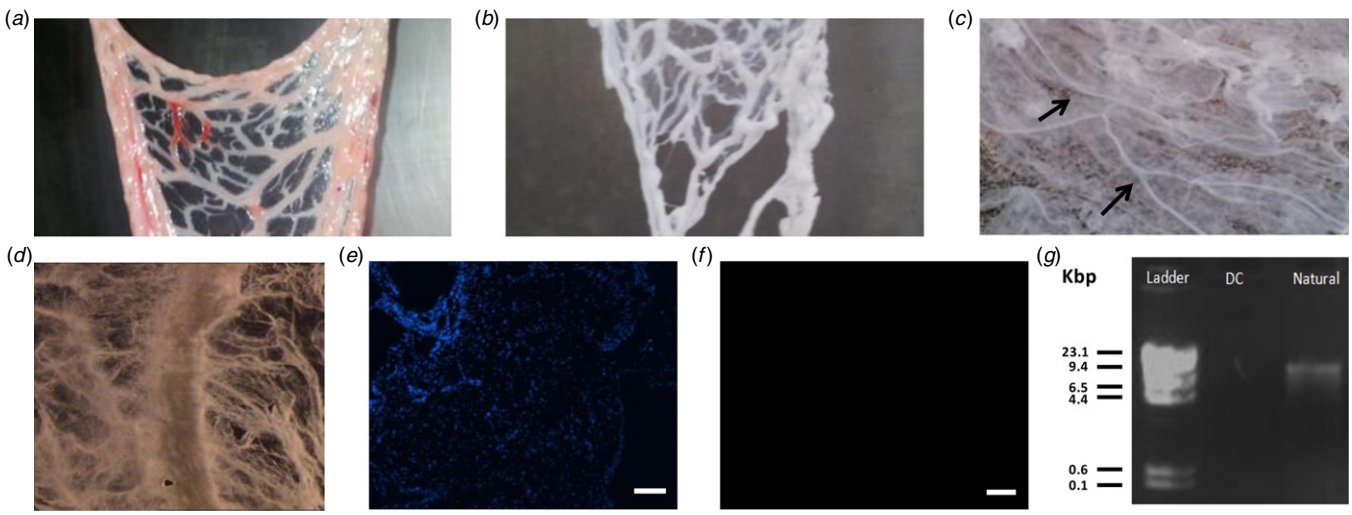

Figure 2. Decellularization process. (*a*) Fresh omentum prior to cell removal. (*b*), (*c*) Omentum during and after complete decellularization. Blood vessel infrastructure is indicated with arrows. (*d*) Higher magnification of the blood vessel infrastructure. (*e*), (*f*) Nuclei staining of fresh (*e*) and decellularized (*f*) omentum (Hoechst 33258; blue). Both images were taken under the same imaging conditions. (*g*) Ethidium bromide DNA gel. Left to right: ladder, decellularized omentum (DC) and fresh omentum (natural). No band associated with the decellularized omentum was found. Bar: $E = 200\ \mu$m, $F = 200\ \mu$m.

We next sought to analyze the composition of the decellularized matrix. Masson's trichrome staining revealed a fibrous, collagen-rich structure (figure 4(*a*)). Immunostaining of the scaffolds revealed high expression of collagen I and IV (figure 4(*b*)) suggesting that the basic fibrous matrix and blood vessel infrastructure was preserved during the

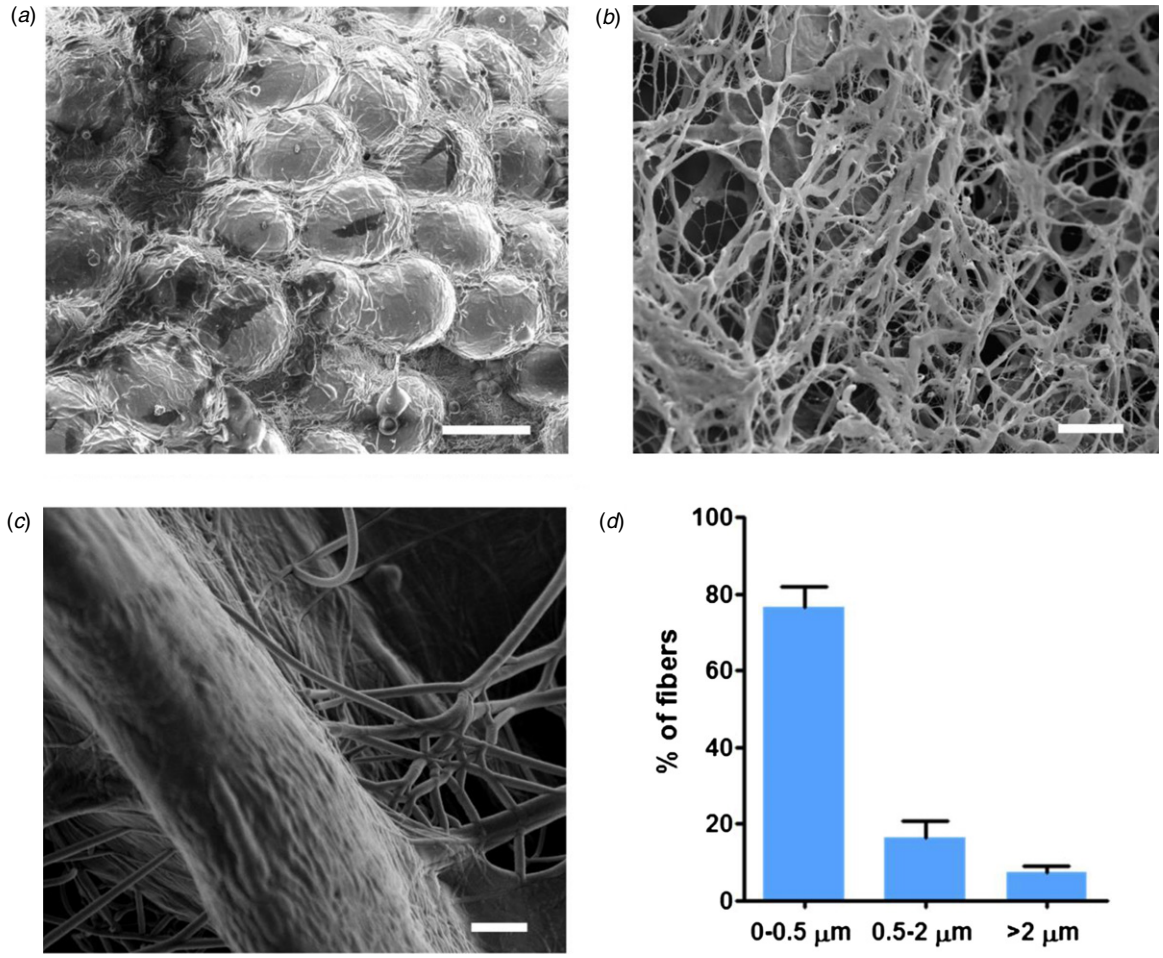

Figure 3. Decellularized matrix analyses. (*a*) SEM image of native omentum. (*b*) SEM image of decellularized omentum. (*c*) HRSEM image of a blood vessel ECM preserved within the decellularized matrix. (*d*) Fiber diameter distribution in the decellularized matrix. Bar: $A = 50\ \mu$m, $B = 20\ \mu$m, $C = 2\ \mu$m.

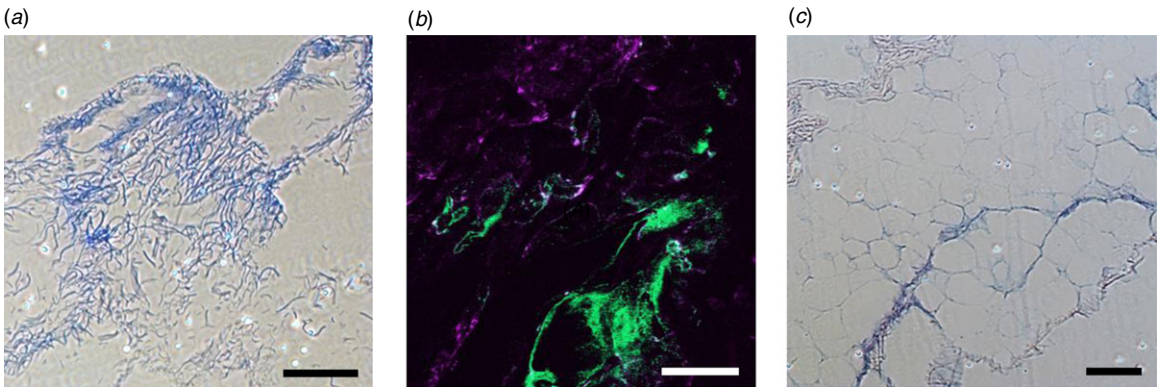

Figure 4. Analyses of matrix components. (*a*) Collagen fibers in the decellularized matrix by Masson's trichrome staining (blue). (*b*) Immunostaining of the decellularized matrix for collagen IV (green) and I (pink). (*c*) GAGs within the decellularized matrix by Alcian blue staining (light blue). Bar: $A = 100\ \mu$m, $B = 50\ \mu$m, $C = 50\ \mu$m.

decellularization process. Further indication of protein content within the decellularized omentum was provided by the mass spectrometry (MS) proteomic analysis. Among the collagen proteins in the matrix we identified mostly structural collagenous proteins, such as collagen types I and III, which provide mechanical support to the matrix, collagen type II which interacts with proteoglycans and provides tensile strength to tissues and collagen type V, associated with initiation of collagen fibril assembly [48]. Furthermore, collagens IV and VI, comprising the basement membrane of

blood vessels were also detected, providing additional support that the basic building blocks of blood vessel infrastructure were preserved.

In addition to their capacity to bind water and thus form hydrated matrices, sulfated GAGs can electrostatically bind heparin binding proteins and control their release into the cellular microenvironment. Therefore, we next evaluated the existence of these molecules after tissue processing. GAGs preservation within the decellularized omentum matrix was qualitatively detected by Alcian blue staining (figure 4(*c*)). Using Blyscan assay, 1.7 μg of sulfated GAGs were found in 1 mg dry matrix. Further optimization of the decellularization process should be performed in order to increase GAG content in the matrix. In theory, these molecules can serve as controlled release systems for various growth factors essential for engineering vascularized cardiac patches, including IGF-1 and VEGF, promoting cardioprotection and vascularization, respectively [12].

A prerequisite from matrices for cardiac tissue engineering is to withstand the physiological working conditions of the heart. To evaluate whether the mechanical properties of the decellularized omentum may support cardiac function, we analyzed the matrix by three mechanical assays: cyclic-strain, strain-relaxation and strain-to-break. Representative graphs are presented in supporting information (figure S2, available at stacks.iop.org/BF/6/024101/mmedia). We found that the scaffolds exhibited low hysteresis and high elasticity, as evident by the distance between the ascending and descending curves in the cyclic-strain assay. Almost no reduction of peak stress values for consequent cycles or reduction of minimum stress at starting point was observed in the omental scaffolds (figure S2A). Although the omental scaffolds exhibited, as expected, lower ultimate strength than the cardiac ECM, both the omental and cardiac ECM had initial failure at 20% stretch in the strain-to-break assay (figure S2B), suggesting a potential to withstand physiological strain (i.e. $<$20%) after transplantation [49]. In the stress-relaxation assay, the omental scaffolds exhibited viscoelastic behavior (figure S2C), resembling to previously described stress-relaxation results of native heart tissue [50].

2.3. Engineering functional cardiac patches

Next, we assessed the potential of the matrices to support cardiac cell culture and tissue assembly over time. Cardiac cells were isolated from the ventricles of neonatal rats and seeded with a single droplet into the matrices (figure 5(*a*)). Cell viability was assessed over time by live/dead staining and XTT viability assay, revealing negligible cell death and maintenance of viability throughout the cultivation period (figures 5(*b*) and (*c*)). As cardiomyocytes do not proliferate *in vitro*, the slight increase in cell number may be attributed to the proliferation of cardiac-fibroblast, left in the culture after the pre-plating process.

To evaluate cardiac cell morphology within the scaffolds, the constructs were double stained for troponin I and collagen I. Confocal images of cell-seeded constructs on day 3, revealed that the cells are located on the collagen fibers

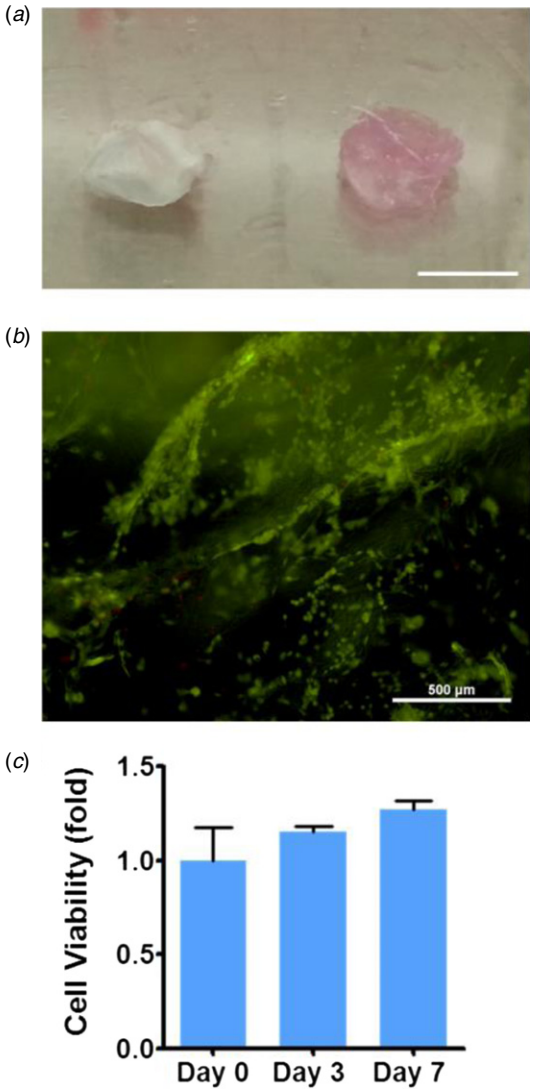

Figure 5. Cardiac cell seeding and viability. (*a*) The omental scaffold prior (left) and after (right) cell seeding. Bar = 5 mm. (*b*) Live/dead assay on day 7. Bar = 500 μm. Green and red represent live and dead cells, respectively. (*c*) XTT viability assay.

(pink), suggesting cell–matrix interaction (figure 6(*a*)). On day 7, the cells assembled into elongated and aligned cell bundles (figures 6(*b*) and (*c*)). Analysis of cardiomyocyte morphology revealed aspect ratio of 4.8 $\pm$ 0.44. sarcomeric α-actinin (pink) staining revealed massive striation, indicating the contraction potential of the tissue (figure 6(*c*)) with morphology similar to that of cells cultivated on decellularized heart (figure 6(*d*)), or in the myocardium [10]. High resolution SEM (HRSEM) images of cardiac cells grown within the omental matrix provided further indication for cell elongation and alignment, and for cell–cell and cell–matrix interactions (figure 6(*e*)). We noticed that during the cultivation period the pores of the matrices were gradually filled, probably with ECM proteins secreted by cardiac-fibroblasts (figure 6(*f*)).

Since a strong contraction of the engineered tissue is essential for creating an effective heart patch [2, 15], we evaluated the spontaneous contraction amplitude and rate of the engineered patches. As shown, both of the parameters were at the same order of cardiac tissue engineered within

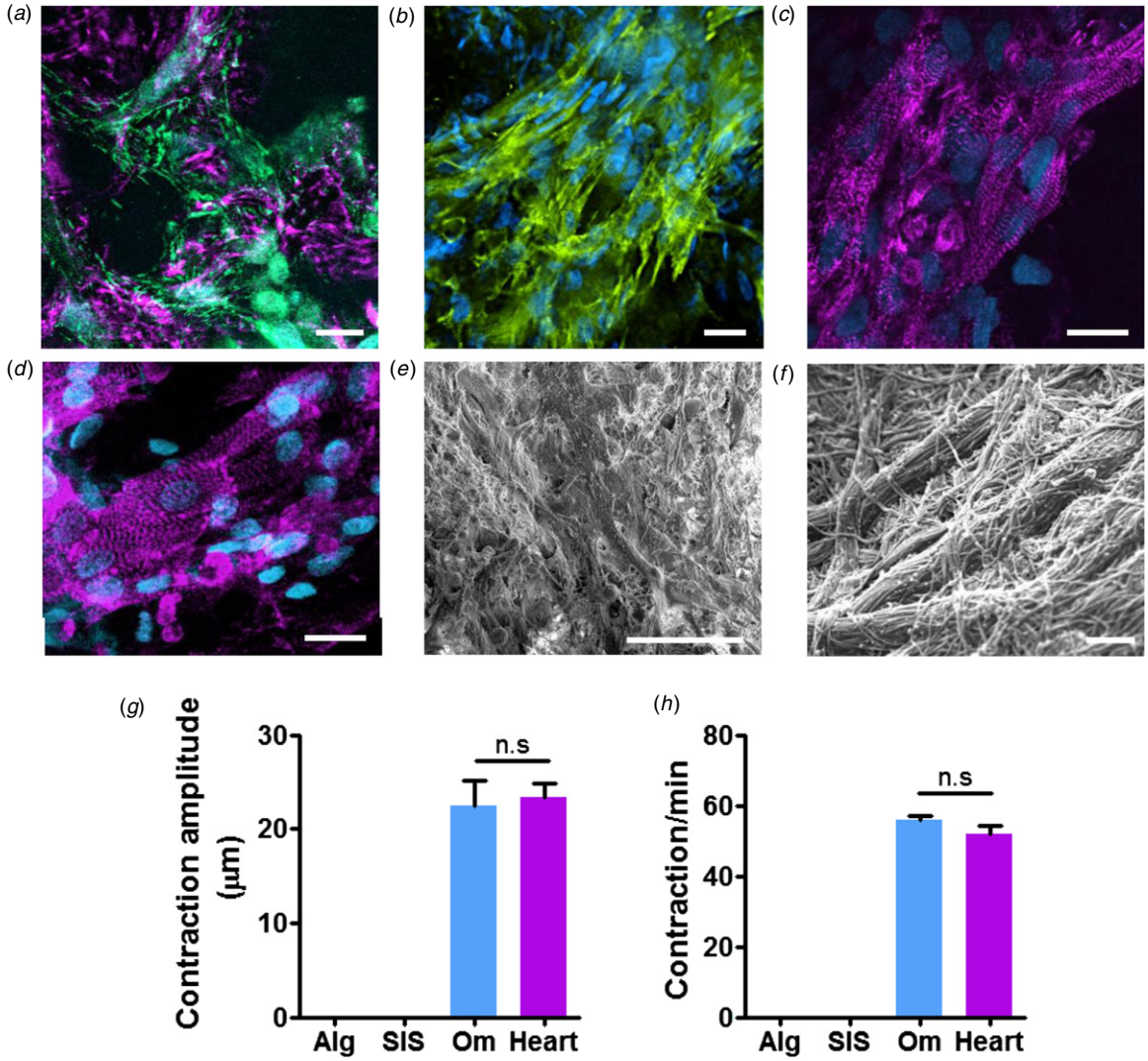

Figure 6. Cardiac tissue assembly and function. (*a*) Cardiac cell assembly on omental matrix fibers as judged by troponin I (green) and collagen I (pink) staining on day 3. (*b*) Troponin I staining of cardiac cells on day 7. (*c*), (*d*) Cardiac α sarcomeric actinin staining on day 7 of cardiomyocytes within the omentum matrix (*c*) and decellularized heart matrix (*d*). (*e*) HRSEM image of cardiac cell elongation on the matrix on day 7. (*f*) ECM proteins secreted by the cultured cardiac cells on day 7, decreasing pore size. (*g*), (*h*) Engineered tissue function on day 3. (*g*) Contraction amplitude. (*h*) Contraction rate. Engineered tissues within the omental matrix (Om), heart matrix (Heart), porcine small intestine submucosa scaffold (SIS), and alginate sponge (Alg). Bar: $A = 500$ μm, B, C and $D = 20$ μm, $E = 50$ μm, $F = 1$ μm.

decellularized heart matrix (figures 6(*g*) and (*h*)). However, although we used a standard heart decellularization process [14] the use of SDS may have affected heart matrix properties and therefore the contraction of the engineered tissue. Cells seeded onto alginate scaffolds [12] or small intestine submucosa (SIS) membranes [51–53], serving as control groups, were not able to induce construct contraction, although contractions of individual cell aggregates were observed. The absence of full construct contraction of the tissues engineered on the SIS membranes may be attributed to the higher fiber density in these matrices compared to the omental matrices. Higher density leads to higher scaffold weight, hampering the ability of the cells to contract the entire construct.

2.4. Vascularization of the cardiac patch

Prevascularization of the patch is essential for its proper integration with the host myocardium after implantation. In the absence of proper vasculature, following transplantation, oxygen cannot reach the implanted cells and the cardiac cells comprising the patch cannot survive [15]. Therefore, we next sought to assess the ability of the omentum-based matrix to induce the assembly of endothelial cells into blood vessels. Human umbilical vein endothelial cells (HUVECs) were seeded on the matrix to form blood vessel networks on the blood vessel infrastructure. As shown, endothelial cells, positively stained for CD31 marker (pink) were located on collagen IV fibers (green) within the matrix, forming tube-like structures (figures 7(*a*) and (*b*)).

Next, HUVECs were co-cultured with cardiac cells at various endothelial:cardiac cell ratios (described in methods section). Structures resembling blood vessel networks (CD31; pink) in-between cardiac cell bundles (troponin I; green) were observed in the different cultures (representative images for 25% endothelial cell ratio are shown in figures 7(*c*) and (*d*)).

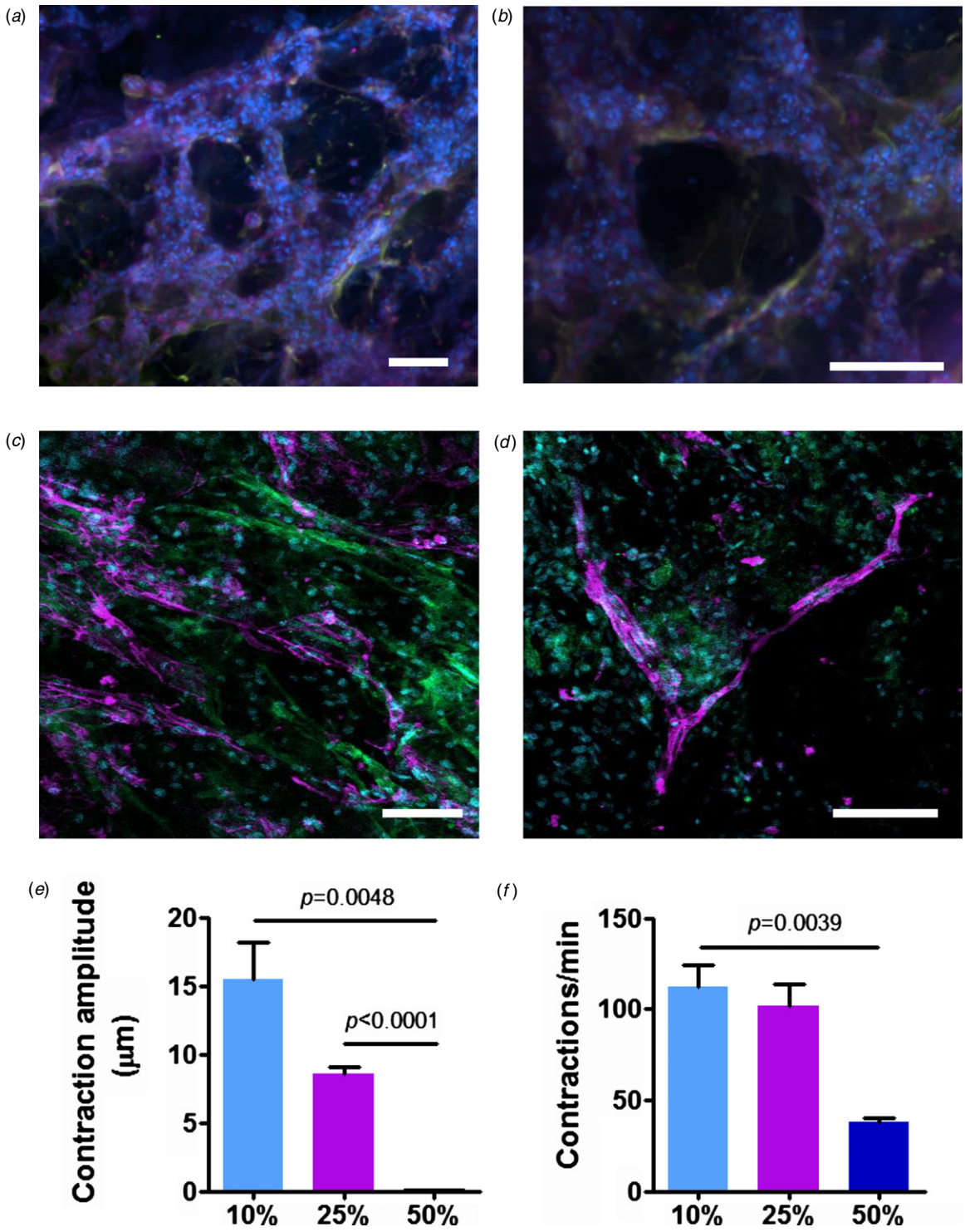

Figure 7. Vascularization of the cardiac patch. (*a*) HUVECs seeded on the matrix, stained for CD31 (pink) located on collagen IV (green) fibers. (*b*) Same image at higher magnification. (*c*), (*d*) Endothelial cells co-seeded with cardiac cells (endothelial cells represent 25% of total cells) on day 7, stained for CD31 (pink) and cardiac troponin I (green). (*e*), (*f*) Contraction amplitude and of the vascularized tissues (day 7), engineered with varying percentages of endothelial cells (10%, 25%, 50%). Bar: $A = 100\ \mu$m, $B = 100\ \mu$m, $C = 100\ \mu$m, $D = 100\ \mu$m.

We then evaluated the contraction properties of the vascularized cardiac patches. As shown in figures 7(*e*) and (*f*), higher contraction amplitude and contraction rate were observed in cardiac patches seeded with higher cardiac cell percentage. We also observed that when the cell constructs were cultured in EGM-2 medium (figure 7(*f*)), the contraction rate was significantly higher than of constructs cultured in M199 medium (figure 6(*h*)). This is probably due to growth factor supplements in the enriched EGM-2 medium (epidermal GF, vascular endothelial GF, basic fibroblast factor, IGF-1). Overall, such prevascularization of a cardiac patch may promote rapid anastomosis with the host blood vessel network,

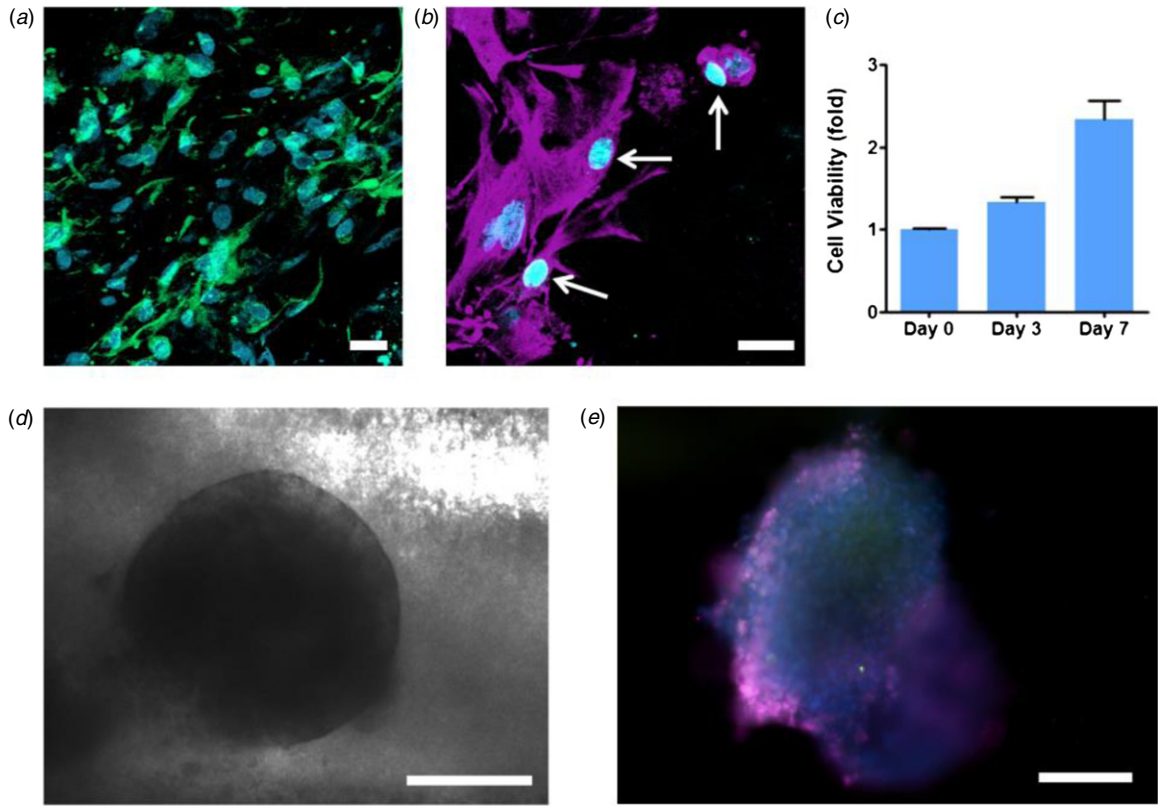

Figure 8. Mesenchymal and iP stem cells growth on the omental scaffold. (*a*) Rat MSCs staining for Sca-1 (green) and nuclei (blue) on day 7. (*b*) Rat MSCs staining for vimentin (pink), Ki-67 proliferation marker (green) and nuclei (blue) on day 7. Arrows indicate Ki67 positively stained cells. (*c*) XTT viability assay of MSCs cultured on omental matrices. Values are fold increase over the initial cell number. (*d*) iPS cells form embryoid bodies when cultured on the omental matrix. (*e*) iPS cells staining on day 7 for SSEA-4 (pink), Nanog (green) and nuclei (blue). Bar: $A = 20\ \mu$m, $B = 20\ \mu$m, $D = 100\ \mu$m, $E = 100\ \mu$m.

allowing proper oxygen and nutrients transfer to the graft and maintenance of cell viability [12, 15, 54].

2.5. Omentum matrix as a platform for engineering autologous tissues

We believe that parts of the omental tissue can be harvested from patients in a relatively simple procedure using microsurgery techniques [42, 43]. After a quick decellularization process, the obtained matrix would be able to serve as an autologous scaffold for growing tissues composed of cells isolated from the same patient. It has been previously shown that mesenchymal stem cell (MSCs) have a therapeutic effect on the infarcted heart both when MSC-based engineered tissues were implanted or when the cells were injected directly into the infarct [55–58]. In addition, the potential of induced pluripotent stem cells (iPS) to differentiate into contracting cardiomyocytes was previously reported [59–61]. Therefore, as a proof of concept, we next sought to evaluate the potential of the matrix to accommodate these cells. The rationale behind these experiments was that both MSCs and iPS cells can be obtained from the patient, manipulated and seeded within the patient's derived matrix. Later the stem cell-comprising patch could be re-transplanted instead of the injured cardiac tissue. This approach may represent a new concept for engineering personalized cardiac patches. MSCs were isolated from rat bone marrow and cultured within omentum matrices. On day 7 the cells exhibited strong staining for stem cell marker Sca-1 (figure 8(*a*), green). Co-staining with vimentin (pink) and Ki67 proliferation marker (green), along with XTT viability assay have indicated cell proliferation within the scaffold (figures 8(*b*) and (*c*)). We further cultured human iPS (hiPS) cells on the omentum matrix. Figures 8(*d*) and (*e*) revealed that seven days after cell seeding, embryoid bodies were formed on the omentum matrix. The cells were positively stained for Nanog (green) and SSEA-4 (pink), indicating that the scaffolds were able to maintain their undifferentiated phenotype without the use of feeder-layer cells. With the proper factors, these cells have been shown to differentiate to cardiomyocytes [59]. These results validate that the combination of the autologous omental matrix with autologous stem cells represents a platform for engineering personalized patches.

3. Conclusions and future prospects

We report the successful decellularization of omental tissue to be used as scaffolds for cardiac tissue engineering. The fibrous scaffold is composed of a micro and nanofiber architecture supporting the cultivated cardiac cells. The matrix is comprised of a dense vascular infrastructure allowing quick vascularization of the patch prior to its transplantation.

Overall, this scaffold promoted the assembly of a vascularized contracting cardiac tissue.

Future studies should focus on further optimization of the decellularization process for better preservation of essential factors within the matrix, such as collagens, GAGs and adhesion molecules. The potential of the matrix to control the release of heparin binding growth factors should also be investigated. More importantly, the ability of this engineered cardiac patch to attenuate the deterioration of the left ventricle after myocardial infarction should be explored in an animal model.

Since several independent groups reported on the existence of stem cells in the omentum, it will be interesting to evaluate the potential of the omentum matrix to control the fate of adult stem cells such as hematopoietic and cardiac stem cells.

4. Materials and methods

4.1. Decellularization of porcine omental tissue

Omenta of healthy six month old pigs were purchased from the institute of animal research in Kibutz Lahav, Israel. Fresh omental tissue was agitated for 1 h in a hypotonic buffer of 10 mM Tris 5 mM ethylenediaminetetraacetic acid (EDTA) and 1 μM phenylmethanesulfonyl-fluoride at pH 8.0. Then the tissue was subjected to three cycles of freezing (−80 °C) and thawing (37 °C) using the same buffer. After the last cycle the tissue was gradually dehydrated by washing it once with 70% ethanol for 30 min and three times in 100% ethanol for 30 min each. Polar lipids of the tissue were then extracted by three 30 min washes of 100% acetone. Subsequently, the a-polar lipids were extracted by three incubations in a 60:40 hexane:acetone solution (8 h each). Then, the defatted tissue was gradually rehydrated and subjected to 0.25% Trypsin–EDTA (Biological Industries, Kibbutz Beit-Haemek, Israel) degradation overnight at room temperature (RT). The tissue was then thoroughly washed with phosphate buffered saline (PBS) and with 50 mM Tris buffer with 1 mM $MgCl_2$ at pH 8.0. Following, the tissue was gently agitated in a nucleic acid degradation solution of 50 mM Tris 1 mM $MgCl_2$ 0.1% bovine serum albumin (BSA) and 40 U ml^{-1} Benzonase® nuclease (Novagen, Madison, WI) at pH 8.0 for 20 h at 37 °C. Finally, the tissue was washed with a buffer containing 50 mM Tris 1% (v/v) triton-X100 (pH 8.0), subsequently with 50 mM Tris buffer (pH 8.0), three times with PBS and three times with sterile double distilled water (DDW). The decellularized tissue was frozen overnight (−20 °C) and lyophilized.

4.2. Decellularization of porcine heart tissue

Hearts of healthy six month old pigs were purchased from the institute of animal research in Kibutz Lahav, Israel. The left ventricle was horizontally cut into 3 mm thick tissue slices and subjected to a decellularization protocol as previously described [14]. Briefly, the tissue was incubated in a lysis buffer (10 mM Tris buffer and 0.1% EDTA, pH 8.0) for 24 hr, followed solubilization in 0.5% sodium dodecyl sulfate (SDS) with orbital mixing (four days, medium was changed every 8 h). Following, the sections were washed in PBS and incubated under orbital mixing with 40 U ml^{-1} Benzonase in 50 mM Tris, 1 mM $MgCl_2$, 0.01% BSA, pH 8.0 at 37 °C for 20 h, washed four times in sterile DDW, frozen overnight (−20 °C) and lyophilized.

4.3. Histology, immunostaining and immunofluorescence

Fresh or decellularized tissues were dehydrated in graduated ethanol steps (70%–100%), fixed in formalin and paraffin-embedded. Sections of 5 μm were obtained and affixed to X-tra® adhesive glass slides (Leica Biosystems). The sections were stained with Masson trichrome (Bio-Optica, Milano, Italy) for cell and collagen detection, and with Alcian blue (Merck, Geneva, Switzerland) for GAG detection.

For immunohistochemistry, heat-mediated antigen retrieval was performed after deparaffinization. Endogenous peroxidases were inhibited by incubating the slides in 3% hydrogen peroxide in PBS for 5 min. Then, the slides were blocked in Dulbecco's modified Eagle Medium (DMEM)-based buffer containing 2% fetal bovine serum (FBS) for 1 h in RT and stained using primary mouse monoclonal anti-human smooth muscle actin antibody (Dako, Glostrup, Denmark) for 1 h in RT. Anti-body labeling was revealed using secondary horseradish peroxidase–conjugated anti-mouse antibody (Dako), visualized using DAB chromogen substrate (Dako).

For immunofluorescence, native, acellular scaffolds or cell-seeded constructs were fixed and permeabilized in cold methanol, blocked for 8 min at RT in Super Block (ScyTek laboratories, West Logan, UT). After three PBS washes, the samples were incubated with primary antibodies: mouse monoclonal anti-collagen I (Sigma, St Louis, MO), rabbit polyclonal anti-collagen 4 (Abcam, Cambridge, MA), rabbit polyclonal anti laminin (Abcam), mouse monoclonal anti VEGF (Abcam), primary rabbit polyclonal anti cardiac troponin I (Abcam), mouse monoclonal anti α-actinin (Sigma), rabbit anti connexin 43 (Invitrogen, Carlsbad, CA), mouse monoclonal anti CD31 (Abcam), rabbit monoclonal anti Ki67 (Abcam), rabbit polyclonal anti Sca-1 (Millipore), mouse anti-Vimentin (Invitrogen), mouse anti SSEA-4 (R&D Systems, Minneapolis, MN), rabbit anti Nanog (Peproteck, Rocky Hill, NJ). After incubation, the samples were washed and incubated for 1 h at RT with secondary antibodies: goat anti-rabbit Alexa Fluor 488 (Jackson, West Grove, PA), Goat Anti-Mouse Alexa Fluor 647 (Jackson). For nuclei detection, the cells were incubated for 5 min with 5 μg ml^{-1} Hoechst 33 258 (Sigma).

Samples were analyzed using a confocal microscope LSM 510 Meta (Zeiss, Germany) or inverted fluorescence microscope (Nikon Eclipse TI).

4.4. Assessment of matrix components

For nuclei detection native and decellularized tissues were stained with Hoechst 33258. The figures were taken under the same imaging conditions. For DNA quantification, nucleic acids were isolated using the phenol-chloroform method and visualized by ethidiume bromid gel electrophoresis.

Total GAG content was quantified in natural and decellularized tissues using dimethylmethylene blue dye-binding assay (DMMB; Blyscan, Biocolor Ltd, Carrickfergus, UK), with a chondroitin sulphate standard, according to manufactures guideline and normalized to dry weight.

The decellularized samples were analyzed by MS performed by an orbitrap ion-trap mass spectrometer (MS, Thermo Fisher Scientific, Inc.). The MS data was analyzed using the MaxQuant 1.2.2.5 software (Mathias Mann's lab, Maxplanq institute) searching against the pig part of the NCBI-nr database.

4.5. Scanning electron microscopy

Cells were fixed by 2.5% gluteraldehyde in PBS for 1 h at RT. After fixation cultures were rinsed with PBS and treated with Guanidine-HCl:Tannic acid (4:5) solution (2%) for 1 h at RT. Cultures were rinsed again with PBS and incubated in 2% OsO_4 solution in PBS for 1 h. Cultures were then washed and dehydrated in graded series of ethanol (50%, 70%, 80%, 90% and 100%). Finally, the preparations were sputtered with gold for SEM (JSM 840A, JEOL) examination, or with carbon for HRSEM examination (Magellan 400L, FEI, Hillsboro, OR, USA).

4.6. Mechanical properties of decellularized scaffolds

Three uniaxial mechanical assays (cyclic-strain, stress-relaxation, and strain-to-break) were conducted on decellularized heart and omentum samples using an Instron universal loading frame, model 5582 universal testing instrument with a 100N load cell. Device control, data acquisition and processing were performed with BlueHill 2.0 materials testing software (Instron). The specimens were hydrated with PBS (pH 7.4) at ambient temperature throughout the testing. *Cyclic loading*. Samples were preconditioned by ten strain-release cycles. The scaffolds were stretched at a fixed rate of 0.05 mm s^{-1} to 15% strain and then released at the same rate to the starting point. After a 3 min rest at starting point, three more strain-release cycles were performed. *Stress-relaxation*. Samples were stretched rapidly (0.5 mm s^{-1}) to 20% strain and held at constant displacement for 10 min, allowing relaxation of stress. *Strain to break*. Samples were stretched at a rate of 0.05 mm s^{-1} until torn. At least three samples were used for each test.

4.7. Cell isolation and culture

Cardiac cell isolation and culture. The procedure for cell isolation employed in this study was approved by the Animal Care and Use Committee of Tel Aviv university, Israel, research authority L-11-053. Neonatal ventricle myocytes (taken from 1- to 3-day-old Sprague-Dawley rats) were isolated using 6–7 cycles of enzyme digestion, as previously described [10]. Briefly, left ventricles were harvested, minced and cells were isolated using enzymatic digestion with collagenase type II (95 U ml^{-1}; Worthington, Lakewood, NJ) and pancreatin (0.6 mg ml^{-1}; Sigma) in DMEM ($CaCl_2 \bullet 2H_20$ (1.8 mM), KCl (5.36 mM), $MgSO_4 \bullet 7H_2O$ (0.81 mM), NaCl (0.1 M), $NaHCO_3$ (0.44 mM), NaH_2PO_4 (0.9 mM). After each round of digestion cells were centrifuged (600G, 4 °C, 5 min) and re-suspended in culture medium composed of M-199 supplemented with 0.6 mM $CuSO_4 \bullet 5H_2O$, 0.5 mM $ZnSO_4 \bullet 7H_2O$, 1.5 mM vitamin B12, 500 U ml^{-1} penicillin (Biological Industries) and 100 mg ml^{-1} streptomycin (Biological Industries), and 0.5% (v/v) FBS. To enrich the cardiomyocytes population, cells were suspended in culture medium with 5% FBS and pre-plated twice (30 min). Cell number and viability was determined by hemocytometer and trypan blue exclusion assay. 5×10^5 cardiac cells were seeded onto 5 mm diameter scaffolds by adding 10 μl of the suspended cells, followed by 40 min incubation period (37 °C, 5% CO_2). Following, cell constructs were supplemented with culture medium (with 5% FBS) for further incubation. Cardiac cells seeded onto Surgisis SIS scaffolds (Cook Biotech Inc.) [62], or alginate scaffolds, were used as control groups [12, 63]. *HUVECs culture.* HUVECs (passage 4; Lonza, Basel, Switzerland) were cultured in Endothelial cell medium (EGM-2, PromoCell, Heidelberg, Germany). HUVECs and cardiac cells were cultured at various endothelial:cardiac cell ratios (10%, 25% and 50% HUVECs) in EGM-2. *MSC isolation and culture.* MSCs were isolated from the femurs of 4–6 weeks old Sprague-Dawley rats, as previously described [64]. Briefly, cells were aspirated from each bone, seeded separately on culture plates and grown in complete medium (high-glucose DMEM, supplemented with 10% (v/v) FBS, 1% (w/v) penicillin–streptomycin and 1% (w/v) l-glutamine, all materials from Biological Industries). The next day, nonadherent cells were removed by several washes with a fresh warmed medium. MSCs were identified by adherence to the flask. MSCs were allowed to grow to 70% confluence and then harvested, replated, and cultured for an additional week prior to seeding on the omentum scaffold. *hiPSCs culture.* hiPSCs were a kind gift from Professor Lior Gepstein's laboratory, the Technion institute, Haifa, Israel. hiPSCs were removed from the mouse embryonic fibroblast feeder-layer, dispersed into cell-clumps using collagenase type IV (300 U ml^{-1}, Worthington Biochemical Corporation, Lakewood, NJ), seeded onto the omental scaffolds and cultured as previously described [59].

4.8. Assessment of cell viability

Cell viability was determined by a colorimetric XTT assay for the quantification of cell proliferation and viability (Biological Industries) according to the manufacturer's instructions. Then, the absorbance of each sample (475 nm) was measured against a background control (665 nm) using a SynergyHT microplate photometer. *Live/Dead assay*: scaffolds seeded with cardiac cells were subjected to a fluorecein-diacetate (FDA) and propidium iodide (PI) staining assay. Seeded scaffolds were immersed for 20 min in 5 μg ml^{-1} FDA (Sigma) and 4 μg ml^{-1} PI (Sigma) in culture medium at 37 °C. Samples were washed with PBS and imaged using a fluorescence microscope (Nikon Eclipse TI, inverted).

4.9. Analyses of tissue function

Contraction of the cardiac cell constructs was recorded using an inverted microscope. Contraction amplitude was analyzed using ImageJ software (NIH). Contraction rate was counted.

4.10. Statistical analysis

Data are presented as means ± SEM. Univariate differences between the groups were assessed using Student's t-test. All analyses were performed using GraphPad Prism version 5.00 for Windows (GraphPad Software). $P < 0.05$ was considered significant.

Acknowledgment

TD acknowledges support from the European Union FP7 program, Alon Fellowship, and the Nicholas and Elizabeth Slezak Super Center for Cardiac Research and Biomedical Engineering at Tel Aviv University. MS thanks the Marian Gertner Institute for Medical Nanosystems Fellowship. The work is part of the doctoral thesis of MS at Tel-Aviv University. We would like to thank Professor Lior Gepstein for the iPS cells, Koby Baranes for help with SEM, Dr Natalie Landa for assistance with immunohistochemistry and the Smoler Proteomics Center at the Technion, Israel for preparation and analyses of the MS data presented herein.

References

[1] Jawad H, Lyon A R, Harding S E, Ali N N and Boccaccini A R 2008 *Br. Med. Bull.* **87** 31
[2] Vunjak-Novakovic G, Tandon N, Godier A, Maidhof R, Marsano A, Martens T P and Radisic M 2010 *Tissue Eng. B: Rev.* **16** 169
[3] Fleischer S and Dvir T 2013 *Curr. Opin. Biotechnol.* **24** 664–71
[4] Dvir T, Timko B P, Kohane D S and Langer R 2011 *Nature Nanotechnol.* **6** 720
[5] Engelmayr G C Jr, Cheng M, Bettinger C J, Borenstein J T, Langer R and Freed L E 2008 *Nature Mater.* **7** 1003
[6] Dar A, Shachar M, Leor J and Cohen S 2002 *Biotechnol. Bioeng.* **80** 305
[7] Zhang B, Xiao Y, Hsieh A, Thavandiran N and Radisic M 2011 *Nanotechnology* **22** 494003
[8] Zimmermann W H *et al* 2006 *Nature Med.* **12** 452
[9] Zong X, Bien H, Chung C Y, Yin L, Fang D, Hsiao B S, Chu B and Entcheva E 2005 *Biomaterials* **26** 5330
[10] Dvir T, Levy O, Shachar M, Granot Y and Cohen S 2007 *Tissue Eng.* **13** 2185
[11] Dvir T, Timko B P, Brigham M D, Naik S R, Karajanagi S S, Levy O, Jin H, Parker K K, Langer R and Kohane D S 2011 *Nature Nanotechnol.* **6** 720
[12] Dvir T *et al* 2009 *Proc. Natl. Acad. Sci. USA* **106** 14990
[13] Leor J, Aboulafia-Etzion S, Dar A, Shapiro L, Barbash I M, Battler A, Granot Y and Cohen S 2000 *Circulation* **102** III-56
[14] Godier-Furnemont A F, Martens T P, Koeckert M S, Wan L, Parks J, Arai K, Zhang G, Hudson B, Homma S and Vunjak-Novakovic G 2011 *Proc. Natl. Acad. Sci. USA* **108** 7974
[15] Iyer R K, Chiu L L, Reis L A and Radisic M 2011 *Curr. Opin. Biotechnol.* **22** 706
[16] Bosman F T and Stamenkovic I 2003 *J. Pathol.* **200** 423
[17] Hynes R O and Naba A 2012 *Cold Spring Harb. Perspect. Biol.* **4** a004903
[18] Dor Y, Djonov V and Keshet E 2003 *Trends Cell Biol.* **13** 131
[19] Shute J 2011 Glycosaminoglycan and chemokine/growth factor interactions *Heparin—A Century of Progress (Handbook of Experimental Pharmacology* vol 207*)* ed R Lever, B Mulloy and C P Page (Heidelberg: Springer) pp 307–24
[20] Hynes R O 2009 *Science* **326** 1216
[21] Ott H C, Matthiesen T S, Goh S K, Black L D, Kren S M, Netoff T I and Taylor D A 2008 *Nature Med.* **14** 213
[22] Eitan Y, Sarig U, Dahan N and Machluf M 2010 *Tissue Eng. C: Methods* **16** 671
[23] Hoshiba T, Lu H, Kawazoe N and Chen G 2010 *Expert Opin. Biol. Ther.* **10** 1717
[24] McFetridge P S, Daniel J W, Bodamyali T, Horrocks M and Chaudhuri J B 2004 *J. Biomed. Mater. Res.* A **70** 224
[25] Yang B, Zhang Y, Zhou L, Sun Z, Zheng J, Chen Y and Dai Y 2010 *Tissue Eng. C: Methods* **16** 1201
[26] Baptista P M, Siddiqui M M, Lozier G, Rodriguez S R, Atala A and Soker S 2011 *Hepatology* **53** 604
[27] Uygun B E *et al* 2010 *Nature Med.* **16** 814
[28] Badylak S F, Taylor D and Uygun K 2011 *Annu. Rev. Biomed. Eng.* **13** 27
[29] Wainwright J M, Czajka C A, Patel U B, Freytes D O, Tobita K, Gilbert T W and Badylak S F 2010 *Tissue Eng. C: Methods* **16** 525
[30] Badylak S F, Freytes D O and Gilbert T W 2009 *Acta Biomaterialia* **5** 1
[31] Collins D, Hogan A M, O'Shea D and Winter D C 2009 *J. Gastrointest. Surg.* **13** 1138
[32] Platell C, Cooper D, Papadimitriou J M and Hall J C 2000 *World J. Gastroenterol.* **6** 169
[33] Shichijo S and Masuda H 1980 *Int. J. Biochem.* **11** 501
[34] Shah S *et al* 2012 *PloS one* **7** e38368
[35] Garcia-Gomez I, Goldsmith H S, Angulo J, Prados A, Lopez-Hervas P, Cuevas B, Dujovny M and Cuevas P 2005 *Neurol. Res.* **27** 807
[36] Singh A K, Patel J, Litbarg N O, Gudehithlu K P, Sethupathi P, Arruda J A and Dunea G 2008 *Cell Tissue Res.* **332** 81
[37] Shrager J B, Wain J C, Wright C D, Donahue D M, Vlahakes G J, Moncure A C, Grillo H C and Mathisen D J 2003 *J. Thorac. Cardiovasc. Surg.* **125** 526
[38] Patel R S and Gilbert R W 2009 *Curr. Opin. Otolaryngol. Head Neck Surg.* **17** 258
[39] Zhang Q X, Magovern C J, Mack C A, Budenbender K T, Ko W and Rosengart T K 1997 *J. Surg. Res.* **67** 147
[40] Milleo F Q, Campos A C, Santoro S, Lacombe A, Santo M A, Vicari M R, Nogaroto V and Artoni R F 2011 *Clinics* **66** 1227
[41] Thorne A, Lonnqvist F, Apelman J, Hellers G and Arner P 2002 *Int. J. Obes. Relat. Metab. Disord.* **26** 193
[42] Merenda M, Litarski A, Kabzinski P and Janczak D 2013 *Pol. Przegl. Chir.* **85** 323–8
[43] Abe T, Kajiyama K, Harimoto N, Gion T and Nagaie T 2012 *Int. J. Surg. Case Rep.* **3** 100
[44] Porzionato A, Sfriso M M, Macchi V, Rambaldo A, Lago G, Lancerotto L, Vindigni V and De Caro R 2013 *Eur. J. Histochem.* **57** e4
[45] Ruvinov E, Dvir T, Leor J and Cohen S 2008 *Expert Rev. Cardiovasc. Ther.* **6** 669
[46] Benedicto H G, Bombonato P P, Macchiarelli G, Stifano G and Prado I M 2011 *Microsc. Res. Tech.* **74** 1018
[47] Robinson T F, Geraci M A, Sonnenblick E H and Factor S M 1988 *Circ. Res.* **63** 577
[48] Gelse K, Poschl E and Aigner T 2003 *Adv. Drug Deliv. Rev.* **55** 1531
[49] Dalen H, Thorstensen A, Aase S A, Ingul C B, Torp H, Vatten L J and Stoylen A 2010 *Eur. J. Echocardiogr.* **11** 176

[50] Sarig U, Au-Yeung G C, Wang Y, Bronshtein T, Dahan N, Boey F Y, Venkatraman S S and Machluf M 2012 *Tissue Eng. A* **18** 2125
[51] Badylak S, Obermiller J, Geddes L and Matheny R 2003 *Heart Surg. Forum* **6** E20–E26
[52] Rosen M, Roselli E E, Faber C, Ratliff N B, Ponsky J L and Smedira N G 2005 *Surg. Innov.* **12** 227
[53] Hata H, Bar A, Dorfman S, Vukadinovic Z, Sawa Y, Haverich A and Hilfiker A 2010 *Eur. J. Cardiothorac. Surg.* **38** 450
[54] Lovett M, Lee K, Edwards A and Kaplan D L 2009 *Tissue Eng. B: Rev.* **15** 353
[55] Nunes S S, Song H, Chiang C K and Radisic M 2011 *J. Cardiovasc. Translational Res.* **4** 592
[56] Miyahara Y *et al* 2006 *Nature Med.* **12** 459
[57] Hatzistergos K E *et al* 2010 *Circ. Res.* **107** 913
[58] Pittenger M F and Martin B J 2004 *Circ. Res.* **95** 9
[59] Itzhaki I *et al* 2011 *Nature* **471** 225
[60] Miki K, Uenaka H, Saito A, Miyagawa S, Sakaguchi T, Higuchi T, Shimizu T, Okano T, Yamanaka S and Sawa Y 2012 *Stem Cells Translational Med.* **1** 430
[61] Zwi-Dantsis L and Gepstein L 2012 *Cell. Mol. Life Sci* **69** 3285
[62] Koffler J, Kaufman-Francis K, Shandalov Y, Egozi D, Pavlov D A, Landesberg A and Levenberg S 2011 *Proc. Natl. Acad. Sci. USA* **108** 14789
[63] Shapiro L and Cohen S 1997 *Biomaterials* **18** 583
[64] Lennon D P and Caplan A I 2006 *Exp. Hematol.* **34** 1606